ORIGINAL PAPER

Andrzej S. Baranski · Piotr M. Diakowski

Application of AC impedance techniques to Scanning Electrochemical Microscopy

Abstract Fundamental aspects of alternating current Scanning Electrochemical Microscopy (AC-SECM) have been studied. In particular, the flow of AC currents in the cell and simplified equivalent circuit diagrams are discussed. In the case of conductive substrates, the local (1st and 2nd order) impedance characteristic of the substrate is presented as a function of DC potential. 3-D imaging of mixed substrates (containing both conductive and non-conductive areas) was performed in the supporting electrolyte alone, without an added redox mediator.

Keywords Scanning electrochemical microscopy · AC-SECM · 2nd order impedance · 2nd harmonic AC voltammetry

Introduction

Scanning Electrochemical Microscopy (SECM) was introduced by Bard [1] 15 years ago. In this technique, a mobile ultramicroelectrode is used to scan an interface in an electrolyte solution at distance comparable to the ultramicroelectrode radius. The main use for Scanning Electrochemical Microscopy is for the imaging of interfacial topography and electrochemical reactivity [2, 3]. Studied systems include metal/solution, semiconductor/solution, liquid/liquid, and liquid/gas interfaces, as well as materials of biological significance. Also very important are the applications of this technique to fundamental studies of electrochemical kinetics [4, 5] and to

A. S. Baranski (✉) · P. M. Diakowski
Department of Chemistry, University of Saskatchewan,
110 Science Place, Saskatoon, SK, S7N 5C9, Canada
E-mail: baranski@duke.usask.ca
Tel.: +1-306-9664701
Fax: +1-306-9664730

chemical analysis [6, 7]. In recent years, a growing number of applications of SECM in corrosion studies have also been observed [8].

SECM measurements are typically carried out in a DC amperometric mode. A redox species added into solution produces a current at the mobile ultramicroelectrode; that current changes in proximity to the studied interface, providing rich information about the topography and reactivity of that interface. SECM measurements can also be carried out under AC amperometric conditions. The theoretical basis of such measurements was given by Horrocks et al [9] but since then only a few papers in this area have appeared in the literature. Alpuche-Aviles and Wipf [10] used AC impedance to generate a feedback signal for scanning electrochemical microscopy, but they monitored changes in the impedance caused by a faradaic process of a redox couple added to the studied solution, so, in fact, their feedback control was very similar to one used in classical SECM measurements. Schuhmann and coworkers [11, 12, 13] showed for the first time that under AC conditions SECM imaging can be performed without any redox mediator present in solution. Bringing the electrode tip nearer to the surface of a non-conductive substrate causes an increase in the electrode impedance (due to a change in the solution resistance), and in the case of conductive substrates the trend, in general, is the opposite (although complicated by the interfacial properties of the conductive surface under the tip). In their most recent paper, Etienne et al. [13] described an elegant method that allows the imaging of mixed substrates (containing conductive and nonconductive areas) to a very high resolution under alternating current conditions. We have worked on the development of AC impedance Scanning Electrochemical Microscopy for the last four years, and although some of our ideas are similar to those already described by Schuhmann and coworkers [11, 12], but, in general, our approach has been somewhat different. We are primarily interested in the monitoring of local interfacial reactivity of conductive substrates; for that reason it was important for us to

control the substrate potential. Typically, we work with a four-electrode system (rather than the two-electrode system described in the cited papers). In addition, we are interested in localized second-order impedance phenomena such as second harmonic generation and faradaic rectification [14].

Materials and methods

Reagents

All solutions were prepared in double-distilled deionized water (Corning Mega-Pure System, MP-6A and D-2) using ACS grade chemicals. $Ru(NH_3)_6Cl_3$ was purchased from Alfa Aesar. All electrochemical measurements were carried out without the removal of dissolved oxygen.

Working electrodes were prepared by sealing Pt wires (Alfa-Aesar) into Corning Kovar Sealing glass tubing #7052 (World Precision Instruments). A lead was made by connecting copper wire with a micro-wire using a silver conductive adhesive paste (Alfa Aesar). The tip of the electrode was conically sharpened with the aid of a rotating carborundum disk (600 grade). The RG parameter (the ratio between the outer diameter of the insulating glass sheath and the diameter of platinum wire) was 8–10. The surface of the working electrode was polished with 3 μm and 0.3 μm aluminum oxide finishing films (TrueView Products Inc). The size of all disk electrodes used in this work is described in terms of their diameter.

A bimetallic (Pt/Au) base electrode was prepared by electrodeposition (constant current) of gold from $KAu(CN)_2$ solution onto 100 μm Pt wire. After the desired thickness of the gold layer was reached, the wire was visually inspected and annealed in an oven (Lindberg) at 1000 °C to smoothen the gold layer. Next, the wire was sealed under vacuum into a low melting point glass capillary tube. The sealed capillary was then cut perpendicular to its length and an electrical connection was made to the unsealed end of the Pt wire. A capillary prepared in this way was mounted vertically into a plexiglass plate using an optical adhesive (Norland, NJ, USA). The upper side of the plate was polished flat to expose the platinum disk/gold ring electrode.

Most experiments were carried out with a tungsten wire used as a pseudoreference electrode; however, all potentials in this paper are reported versus the standard Ag/AgCl electrode.

SECM apparatus

A MX760R motorized micromanipulator (SD Instruments, USA) was used as a positioning/scanning device. This micromanipulator employs four DC motors (X, Y, Z and tilt axis) in conjunction with motor encoders, and is capable of moving in 0.1 μm increments. In this study only three, the X, Y and Z motors, were used. The micromanipulator was interfaced with a personal computer and controlled via serial port communication. Fine positioning of the tip electrode along the Z axis was obtained by means of a piezoelectric disk translator (P-286.40 from Polytec PI Inc), capable of moving the electrode a maximum distance of 200 μm. The piezoelectric translator was driven by a 16-bit digital-to-analog converter via a high voltage power supply (1A12-N4-C from UltraVolt Inc).

The micromanipulator was mounted onto an aluminum plate and the electrochemical cell was attached to the micromanipulator. The scanning tip was attached to the piezoelectric disk translator and mounted above the electrochemical cell. A fiber optic borescope coupled to a digital camera and a fiber optic illuminator were used to assist in the initial positioning of the tip relative to the sample.

Electrodes were connected to a custom built potentiostat (described below), which was interfaced with a computer. The micromanipulator, electrochemical cell, and tip electrode were housed in a grounded Faraday cage to reduce environmental noise.

Electronic circuit

A custom-built electronic system was used to control the micromanipulator and to perform all necessary data acquisition functions. The system was based on two microcontrollers (Microchip PIC18F452) that were interfaced with a computer via a serial link. The current was sampled with a 16-bit analog-to-digital converter (Texas-Instruments TLC4545) after passing through an anti-aliasing filter made of a clock-tunable fifth-order Bessel low pass filter (Linear LTC1065). The system was also equipped with several 16- and 12-bit digital-to-analog converters that were used to control the potentiostat, the piezoelectric translator and the motors.

The four-electrode potentiostat used in this work is shown in Fig. 1. This is a classical design [15] where the working (tip) electrode is at virtual ground potential and the potential waveform is applied to the solution via auxiliary and reference electrodes. Here a 12-bit digital-to-analog converter (DAC1) is used to control a DC potential bias of the tip electrode and DAC2 is used to produce an AC sinusoidal modulation with frequency ranging from 0.1–15 kHz. An operation amplifier OPA3 driven by a 12-bit digital-to-analog converter (DAC3) is used to control the potential of the base electrode. In this configuration, the potential of the base versus the reference electrode potential is given by the difference $E_T - E_{OPA3}$ (where E_T is the tip electrode potential measured versus the reference electrode and E_{OPA3} is the output of the operational amplifier OPA3 measured versus ground). Note that the potential of the base is controlled even if the tip electrode is disconnected from the circuit. The operational amplifier OPA4 is used as a current follower to monitor the passage of current through the tip electrode.
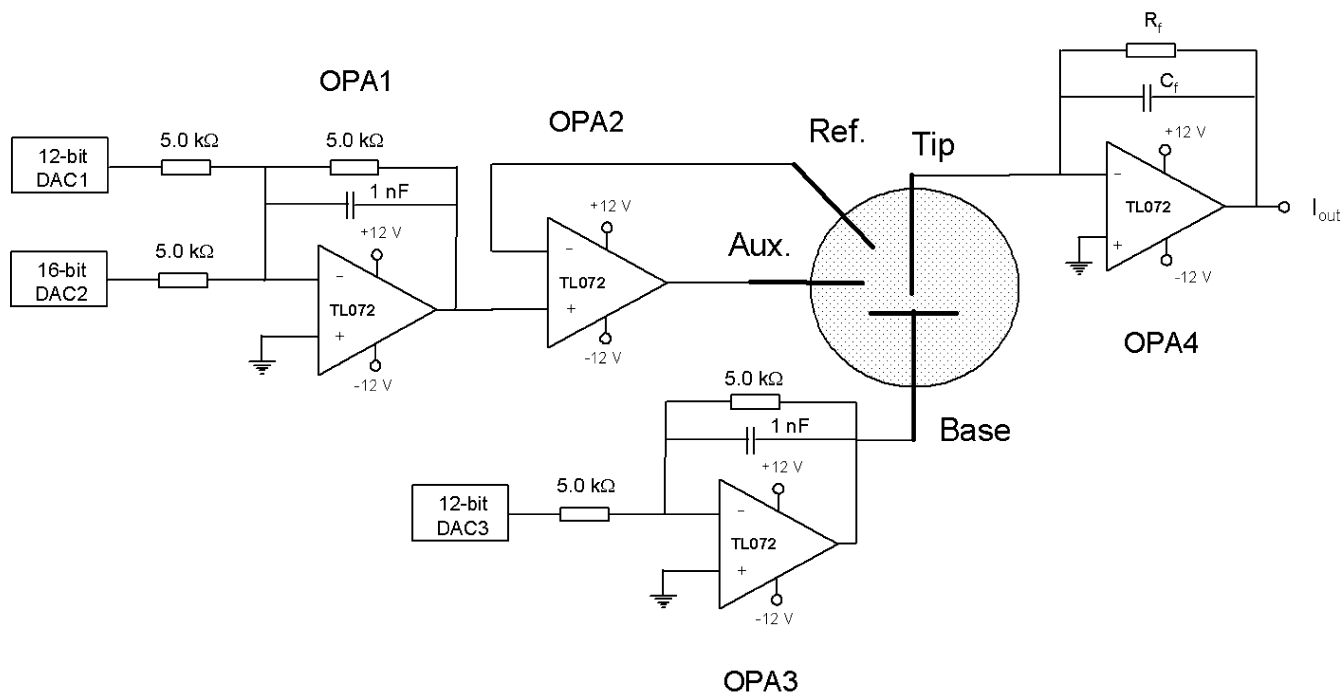
Fig. 1 Four-electrode potentiostat used in most measurements

The bandwidth of all amplifiers (except OPA2) was limited to about 25 kHz. The potentiostat was also equipped with several digitally controlled switches (not shown in the diagram) that were used to change current ranges, connect/disconnect the electrodes, or reverse connections between the tip and the base electrodes.

Impedance data (typically first and second harmonics) were obtained by means of the Fast Fourier Transformation.

The software for the microcontrollers was written in assembly language (with an assembler provided by Microchip), and the PC software (for data acquisition and processing) was written using Microsoft Visual C++ v6.0 and Visual Basic v6.0. The experimental data were further processed in Microsoft Excel; three-dimensional graphs were prepared using Harvard Chart 3.0 graphing software.

Results and discussion

Admittance as a function of distance

In Fig. 2 changes in the absolute admittance of a 25 μm Pt tip electrode as a function of distance from the substrate are shown. The measurements were carried out in $NaClO_4$ solutions with the tip positioned over a plexi-glass (nonconductive substrate) or over a platinum plate (approximately 0.25 cm^2 in surface area). In general, the change in admittance with distance depends on the

Fig. 2 Normalized change in the modulus of the tip electrode admittance as a function of distance from the substrate. (1) non-conductive substrate, (2) not-connected conductive substrate, (3) conductive substrate held at constant potential. Data in **a** were obtained in 1 mM $NaClO_4$ at 3.75 kHz, 350 mV (p-p); data in **b** were obtained in 0.1 M $NaClO_4$ at 468 Hz, 350 mV (p-p)
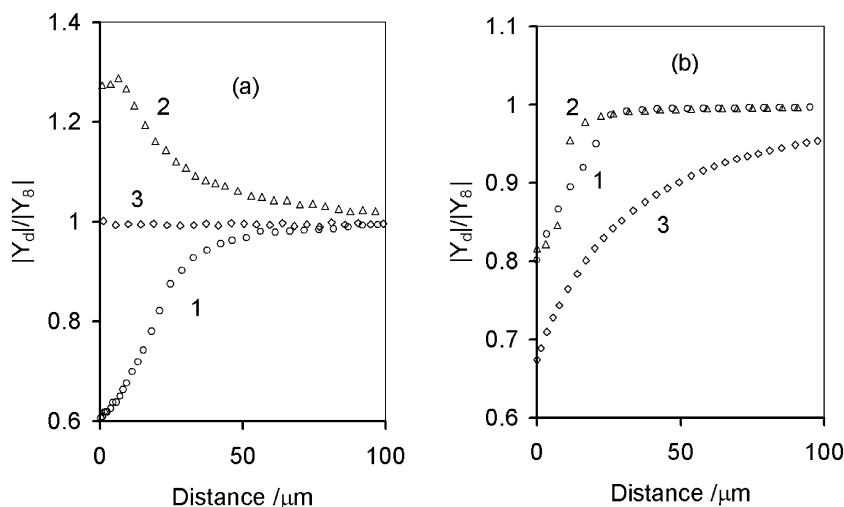
electrical properties of the substrate, concentration of the electrolyte and frequency of the AC modulation. In addition, for conductive substrates, different trends are observed for substrates under potential control and substrates disconnected from the circuit. Figure 2a shows characteristic trends observed in dilute electrolytes at high frequencies; in this case measurements were taken in 1 mM $NaClO_4$ at 3.75 kHz. Measurements were performed with relatively large modulation amplitude (350 mV p-p) to ensure good signal-to-noise ratios. As was recently shown by Engblom et al [16], admittance measurements with large amplitudes are valid.

When the tip approaches a nonconductive surface, the tip admittance decreases (curve 1). The opposite trend is observed when the tip electrode approaches the platinum plate (base electrode) disconnected from the electrical circuit. In this case, the admittance of the tip increases with decreasing distance (curve 2). A similar trend is also observed when the base electrode acts as an auxiliary electrode (such a configuration was earlier studied by Katemann et al [12]). However, when the base electrode is held at a fixed DC potential, the admittance of the tip is practically independent of the distance (curve 3). Trends observed in more concentrated electrolytes and at lower frequencies are shown in Fig. 2b.

In this case, measurements were taken in 0.1 M $NaClO_4$ at 468 Hz. In all three studied cases the admittance of the tip decreases on approach to the surface.

In order to explain the observed behavior let us consider the flow of AC currents in the cell. Diagram A in Fig. 3 represents the tip electrode in proximity to a nonconductive surface and the equivalent circuit for such an arrangement. When the distance between the tip and the surface decreases, the connection between the tip and the auxiliary electrode occurs through a thinner and thinner layer of the solution, so the solution resistance (R_T) increases and the admittance drops.

A somewhat more complicated case involves a tip electrode in proximity to an unconnected base electrode (diagram B in Fig. 3). Here, due to a large interfacial capacitance, the base electrode is AC coupled with the auxiliary electrode. The current from the auxiliary can reach the tip electrode directly through the solution (path i_1) or through the base electrode (path i'_1) by crossing the base electrode/solution interface twice.

In the equivalent circuit Z_{FT} represents the faradaic impedance of the tip, C_T is the double layer capacitance of the tip, R_{TB} is the solution resistance between the tip and the base, C'_B is a part of the double layer capacitance of the base (associated with the surface of the base

Fig. 3 Flow of currents and simplified equivalent circuits for tip electrode in proximity of non-conductive substrate (**A**), tip electrode in proximity of an unconnected base electrode (**B**), and tip electrode in proximity of a base electrode held at constant potential (**C**)
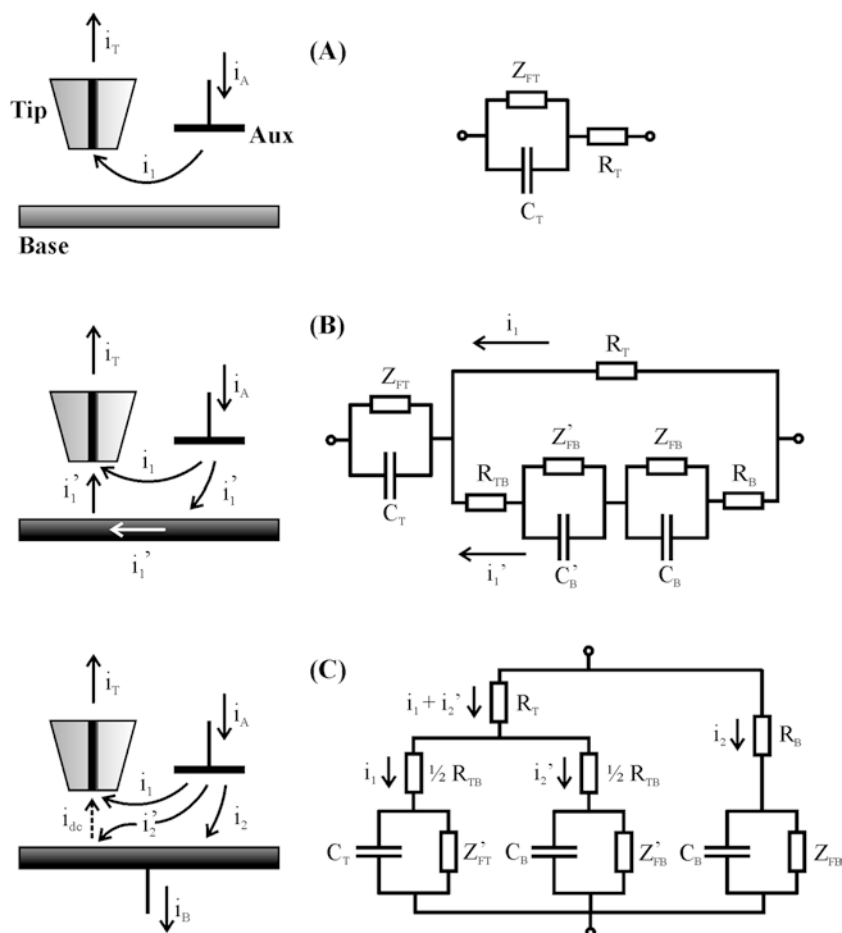
covered by the tip), Z'_{FB} is the faradaic impedance of the base (associated with the surface of the base covered by the tip), C_B is the double layer capacitance of the base (associated with the surface of the base not covered by the tip), Z_{FB} is the faradaic impedance of the base (associated with the surface of the base not covered by the tip), and R_B is the solution resistance of the base electrode. Since the surface area of the base is typically a few orders of magnitude larger than the surface area of the tip, impedances associated with elements C_B, Z_{FB} and R_B are negligibly small, and consequently the admittance of the tip is determined by the interfacial properties of the tip, the interfacial properties of the base (in close proximity to the tip) and the solution resistance which develops between the base and the tip. When the electrolyte concentration is low, the frequency high and the tip electrode relatively large, the impedances of C_T and C'_B may be small in comparison with R_{TB}; in such a case (shown in Fig. 2a, curve 2), the admittance of the tip increases when the tip approaches the surface (because R_{TB} decreases with distance). However, if the impedances of C_T and C'_B are large in comparison with R_{TB} (which takes place at relatively high concentrations and low frequencies), the trend is the opposite (because on the approach to the substrate the impedance of path i_1 increases and the passage of current through path i'_1 is limited by the high impedance of C'_B).

Diagram C in Fig. 3 describes the situation when the tip is in the proximity of a base electrode connected to the output of amplifier OPA3 (see Fig. 1). In this case there is no AC polarization between the base and the tip, so no AC current can flow between these two electrodes; however, a DC current may flow (which is indicated by broken line arrows in the diagram). The AC current passing from the auxiliary electrode can be drained by both the tip and the base electrode. When the tip is very close to the base, the pathways for these two currents (i_1 and i'_2) are almost identical, so in a simplified equivalent circuit diagram we have to consider the interfacial impedances of the tip and the base (covered by the tip) to be connected in parallel. All symbols have the same meaning as before; however, the solution resistance of the tip R_T can be more strictly defined as the resistance of the pathway connecting the middle point, lying between the tip and the base, with the reference electrode. R_T increases as the distance between the tip and the base decreases (similar to the case in diagram A) and R_{TB} decreases as the distance between the tip and the base decreases (similar to the case in diagram B); consequently, in systems where the impedances of C_T and C'_B are small in comparison with R_{TB} (as it is in dilute electrolytes at high frequencies), the admittance of the tip doesn't change much on approach to the surface (curve 3 in Fig. 2a). However, in more concentrated electrolytes and at lower frequencies, when the impedances of C_T and C'_B are large in comparison with R_{TB}, the tip admittance drops when the tip approaches the surface (mainly because of an increase in R_T). More interestingly, the admittance of the tip in such

systems depends on the interfacial properties of the base under the tip, but the coupling is the opposite of the one observed in the case of an unconnected base. Here, when the admittance of the base increases, less AC current flows through the tip and the apparent admittance of the tip decreases. Examples illustrating such behavior are presented in the next section.

We believe that diagram C properly depicts the most important properties of the system, but it also involves very significant oversimplifications. In reality, the two current paths (i_2 and $i_1 + i'_2$) are not totally separate, but rather interconnected through a network of solution resistance elements. In addition, the distribution of current around conductive surfaces is not uniform; consequently, the solution around both electrodes is polarized both vertically and horizontally. It should be emphasized that rigorous circuits for such systems cannot be represented by a finite number of circuit elements connected in a finite number of points, but rather by a three-dimensional network of an infinite number of infinitely small circuit elements. Nevertheless, the diagrams shown in Fig. 3 may be useful in semi-quantitative considerations.
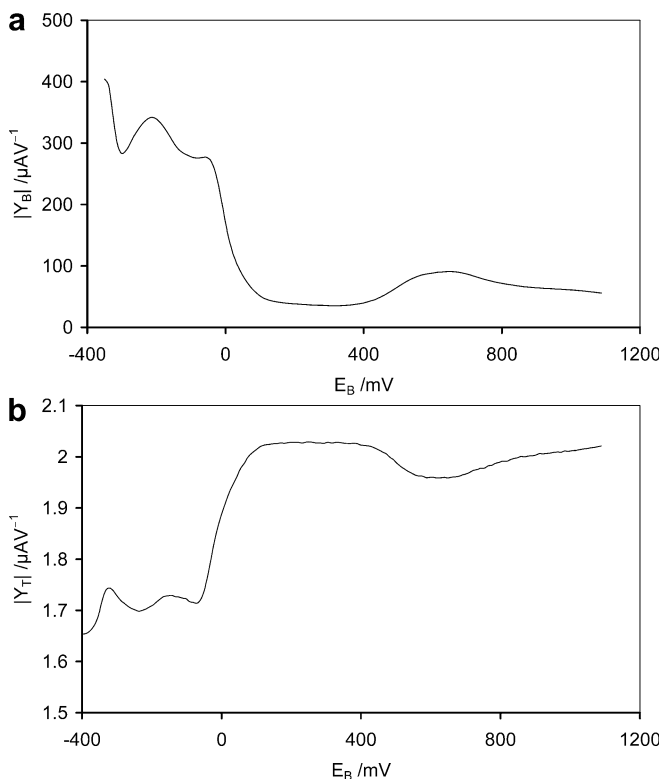
Fig. 4 a Admittance of a 100 μm Pt base electrode versus the base electrode potential observed in 0.1 M H_2SO_4 under standard conditions (three-electrode system). Both AC modulation (936 Hz, 100 mV p-p) and the linear scan were applied to the base electrode. **b** Admittance of a 25 μm Pt tip electrode versus the base electrode potential observed in 0.1 M H_2SO_4 in a four-electrode system. AC modulation (936 Hz, 100 mV p-p) was applied to the auxiliary electrode, the tip electrode held at a constant potential of 800 mV
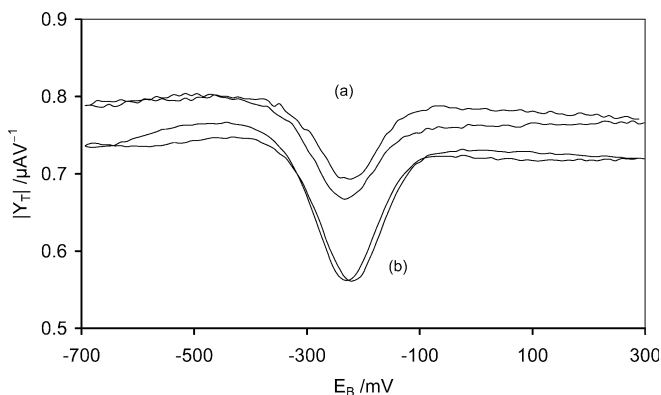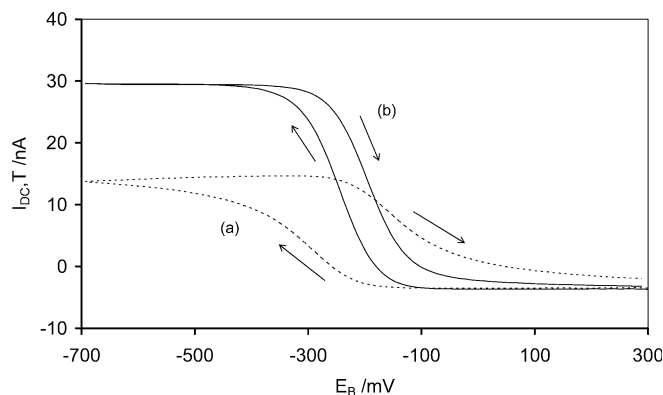
Fig. 5 Admittance of a 25 μm Pt tip electrode versus the base electrode potential observed in a 0.01 M $Ru(NH_3)_6^{3+}$, 0.1 M $(NH_4)_2SO_4$ and 0.1 M NH_3 four-electrode system. AC modulation (936 Hz, 100 mV p-p) was applied to the auxiliary electrode, the tip electrode was held at a constant potential 300 mV, and the linear scan (forward and reversed) was applied to the base electrode. The scan rate was 90 mV/s. The distance between the tip and the base electrode was 46.5 μm for curve (a) and 21.9 μm for curve (b)

## Admittance of the tip as a function of the base electrode potential

All experiments described in this section were carried out with a 25 μm Pt tip electrode positioned above the center of a 100 μm Pt base electrode; both electrodes were sealed in glass. In Fig. 4a, a standard AC voltammogram of the base electrode in 0.1 M H_2SO_4 is shown. The curve was recorded in a standard three-electrode system with the base serving as a working electrode. The tip electrode was about 300 μm above the base and it was disconnected from the circuit. The curve was recorded by changing potentials from negative to positive values. The two overlapping peaks at negative potentials are due to hydrogen desorption, and the hump occurring at about 600 mV is due to platinum oxide formation.

This measurement was repeated in a four-electrode system; this time the tip electrode was positioned 18.2 μm above the base electrode surface. The tip was held at a constant potential (+ 800 mV versus the reference electrode and polarized with an alternating voltage (936 Hz, 100 mV p-p). A potential ramp (from –400 to 1100 mV versus the reference electrode) was applied to the base by means of the circuit shown in Fig. 1. The AC current passing through the tip electrode was monitored and processed by a Fourier Transformation to obtain the admittance. The absolute admittance of the tip electrode plotted as a function of the base electrode potential is shown in Fig. 4b. The shape of the curve is essentially the same as the one shown in Fig. 4a, but the changes of the admittance with potential occur in the opposite direction and the magnitude of these changes is much smaller then in Fig. 4a. This experiment shows that an ultramicroelectrode placed in the proximity of another electrode can sense changes in the interfacial admittance of that electrode and that the description of

Fig. 6 DC current at the tip electrode versus the base electrode potential in 0.01 M $Ru(NH_3)_6^{3+}$, 0.1 M $(NH_4)_2SO_4$ and 0.1 M NH_3 in a four-electrode system. All conditions were the same as in Fig. 5
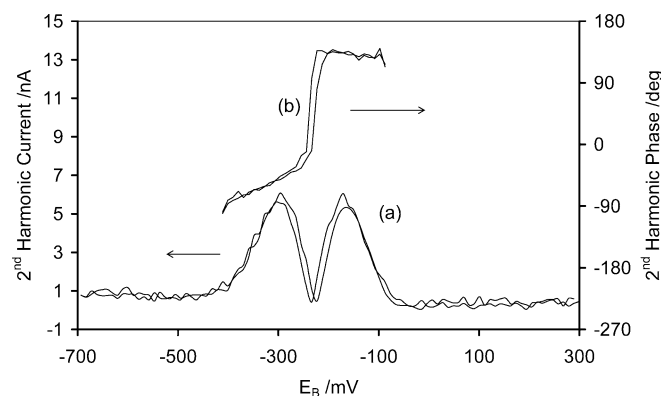
Fig. 7 Modulus of the second harmonic current (a) and the second harmonic phase shift (b) at the tip electrode versus the base electrode potential in 0.01 M $Ru(NH_3)_6^{3+}$, 0.1 M $(NH_4)_2SO_4$ and 0.1 M NH_3 in a four-electrode system. All conditions were the same as in Fig. 5, curve (b)

the phenomenon given in Fig. 3, diagram C is, in principle, correct.

A similar experiment to the one presented in Fig. 4b was also carried out in a solution containing 0.01 M $Ru(NH_3)_6^{3+}$, 0.1 M $(NH_4)_2SO_4$ and 0.1 M NH_3. In this case the observed admittance change is mainly caused by a reversible reduction of the ruthenium complex:

$$Ru(NH_3)_6^{3+} + e^- \rightleftharpoons Ru(NH_3)_6^{2+} \tag{1}$$

Figure 5 shows a decrease in the tip admittance as the base electrode potential crosses the half-wave potential of the $Ru(NH_3)_6^{3+}/Ru(NH_3)_6^{2+}$ redox couple. It should be noted that in this case the tip electrode is held all the time at a constant DC potential of + 300 mV. The figure shows two sets of curves (each containing both forward and reversed scans) obtained for two different positions of the tip electrode above the base electrode surface (46.5 μm for curve a, and 21.9 μm for curve b). As expected, the coupling between the base and the tip electrode becomes stronger as the distance between the two electrodes decreases.

Fig. 8 Three-dimensional image of LP vinyl record grooves. Scanning performed in a feedback mode with a 25 μm Pt tip in 1 mM NaClO$_4$, frequency 890 Hz, amplitude 300 mV (p-p), X and Y step size 10 μm, z_{step} = 5 μm
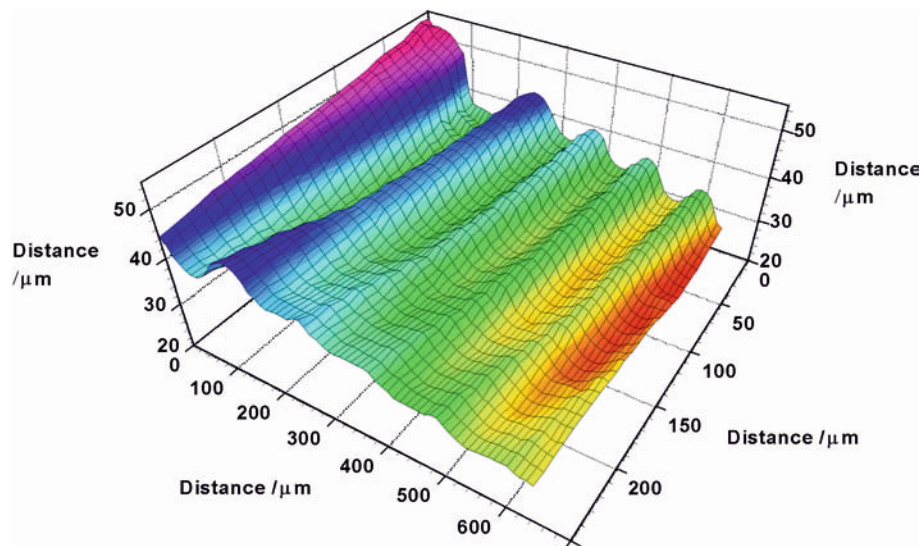
Fig. 9 Change in the modulus of the tip admittance observed during scanning over a platinum gauze sealed in Norland Optical Adhesive. Imaging was performed in a fixed Z mode with a 25 μm Pt tip in 1 mM NaClO$_4$, frequency was 1880 Hz, amplitude was 350 mV (p-p), DC tip potential was −375 mV, X and Y step size was 5 μm
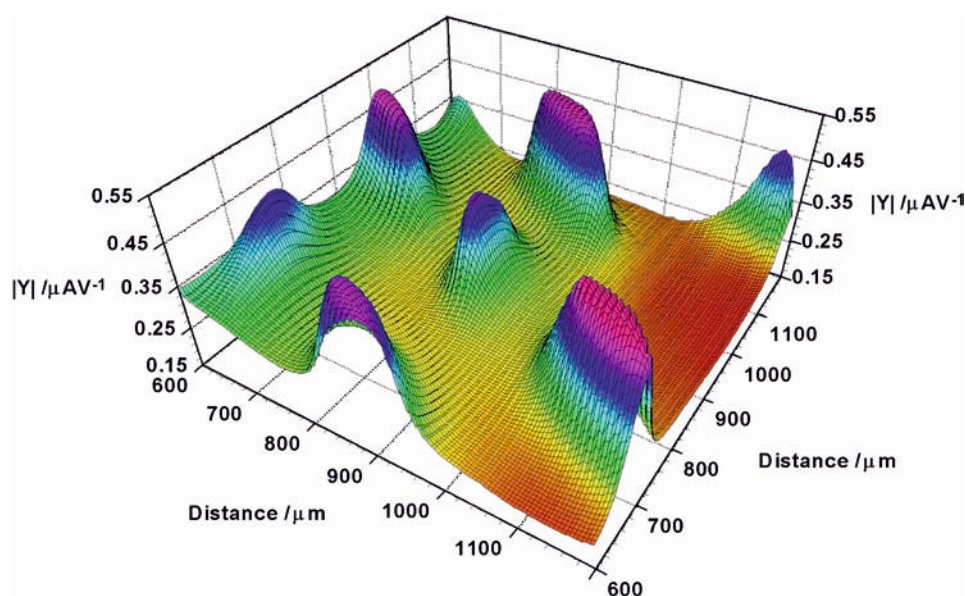
The scanning of the base potential also causes a change in the DC current passing through the tip electrode, as is shown in Fig. 6.

Practically no current is observed when the base electrode is held at potentials more positive then the standard potential of the redox couple, but when the base potential is changed to values more negative than the standard potential, a current step is produced. Here, however, in contrast to Fig. 5, forward and reversed scans do not coincide. The separation between opposite scans increases when the distance between the tip and the base increases. This can be easily explained by the fact that the DC current at the tip electrode is produced by the oxidation of the Ru(NH$_3$)$_6$$^{2+}$ species, which is generated at the base electrode. Of course, it takes some time for the Ru(NH$_3$)$_6$$^{2+}$ species to reach the tip electrode. That delay time could be calculated from Einstein's well-known equation:

$$\Delta t = \frac{d^2}{2D} \tag{2}$$

Here d is the distance between the tip and the base, and D is the diffusion coefficient.

Assuming $D \approx 7 \times 10^{-6}$ cm^2/s, we can calculate Δt as being equal to 0.34 and 1.5 s for the 21.9 and 46.5 μm distances, respectively. These interesting "time-of-flight" phenomena in electrochemical systems were recently studied by Majda and coworkers [17]. Here, however, it is important to emphasize that in the case of the admittance, the forward and reversed scans coincide (when they are plotted as a function of potential) regardless of the distance between the electrodes; clearly the tip electrode can sense a change in the interfacial admittance of the base electrode as it happens – no messenger in the form of a diffusing species is required in this case.
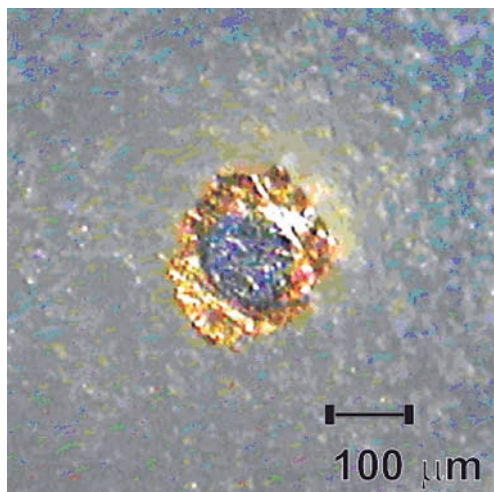
Fig. 10 Photograph of a bimetallic electrode (platinum disk, 100 μm in diameter with a gold ring) sealed in glass

The tip electrode can also sense second harmonic signals generated at the base electrode. Curves shown in Fig. 7 were obtained simultaneously with the curves B shown in Figs. 5 and 6; they are characteristic of a reversible redox process. We also noted that the tip electrode can be used to monitor local faradaic rectification phenomena occurring at the base electrode, but that topic will not be discussed in the present work.

3-D imaging

The fact that the admittance of the scanning tip depends on the distance from the substrate and/or on the interfacial properties of the substrate allows the application of alternating current SECM to the imaging of interfacial topography. The substrate must be surrounded by a dilute electrolytic solution, but in contrast to classical (amperometric) SECM, the presence of a redox species in solution is not required. The imaging is performed by setting several parameters such as sensitivity of the current follower, tip frequency, amplitude and DC bias, as well as parameters controlling the motors (speed and step size for all axes).

The scanning tip is placed about 200–300 μm above the sample surface, and the average tip admittance

Fig. 11 Change in the phase angle of the first harmonic **a** and the modulus of the second harmonic current **b** observed when scanning over a bimetallic electrode (shown in Fig. 10). Imaging was performed in a fixed Z mode with a 25 μm Pt tip in 1 mM NaClO$_4$, frequency was 890 Hz, amplitude was 100 mV(p-p), DC tip potential was 225 mV, X and Y step size was 5 μm. The bimetallic electrode was polarized with 25 mV
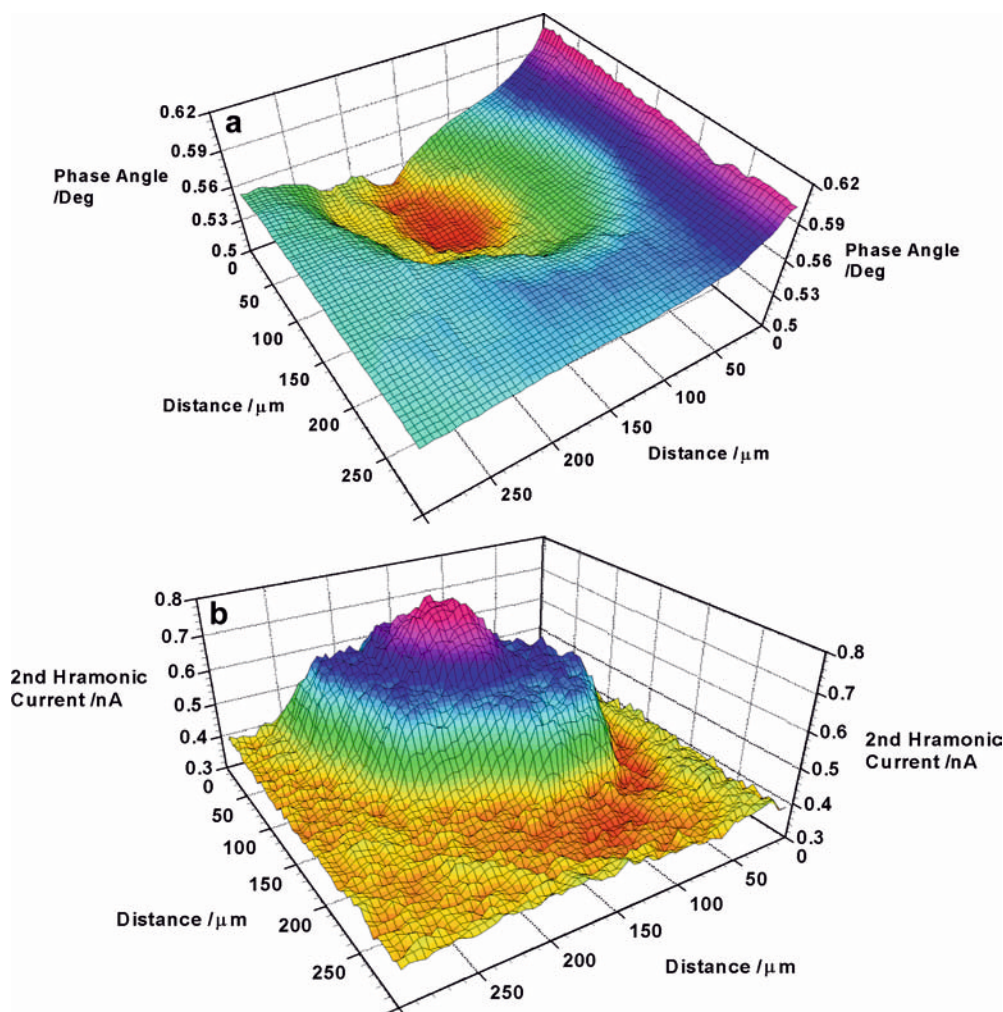
(called the reference admittance, Y_{ref}) and the standard deviation of the admittance Y_{SD} are determined. Next, the tip is moved down by the motor until the tip admittance changes (decreases or increases) by a desired value, ΔY_{max} (typically 30% of Y_{ref}). At that point scanning of the surface begins. Scanning is carried out in roster fashion by changing the X and Y positions in steps. The step size is typically equal to 1/5 of the tip diameter. The imaging is performed in either a feedback or a fixed-Z mode. In the feedback mode, after each step, the Z position is adjusted until the following condition is fulfilled:

$$ABS\left(Y_{X,Y} - Y_{ref}\right) - ABS(\Delta Y_{max}) < 4 \times Y_{SD} \qquad (3)$$

Here $Y_{X,Y}$ is the local tip admittance at position X,Y.

The adjustment of the Z position (ΔZ) is calculated according to the following algorithm:

$$\Delta Z = Z_{step}\left[\frac{ABS\left(Y_{X,Y} - Y_{ref}\right)}{ABS(\Delta Y_{max})} - 1\right] \qquad (4)$$

Here Z_{step} is a constant typically equal to 1/10 of the tip diameter.

The tip is moved up if $ABS(Y_{X,Y} - Y_{ref}) > ABS(\Delta Y_{max}) + 4 Y_{SD}$ and down if $ABS(Y_{X,Y} - Y_{ref}) < ABS(\Delta Y_{max}) - 4 Y_{SD}$; however, if $ABS(Y_{X,Y} - Y_{ref})$ is within $\pm 4 Y_{SD}$ from $ABS(\Delta Y_{max})$, the Z-position of the tip remains unchanged. This feedback procedure works very well in the case of nonconductive substrates. In the case of conductive substrates, the relationship between the admittance and the distance is affected by many factors, and in some systems that relationship is very weak, as is shown in Fig. 2. Conductive substrates and mixed substrates (containing both conductive and non-conductive areas) can be reliably imaged in a fixed-Z mode; in this case, the Z-position of the tip remains constant during the scanning. This scanning mode is also a few times faster than the feedback mode.

The feedback mode was tested by scanning a fragment (650 μm by 300 μm) of a stereo vinyl record placed in a 1 mM solution of $NaClO_4$ with a 25 μm Pt tip electrode. The AC modulation had a frequency of 890 Hz and an amplitude of 300 mV (p-p). The step size in the X and Y directions was 10 μm and Z_{step} was 5 μm. The 3-D image of the vinyl record surface is shown in Fig. 8. This figure clearly demonstrates that monitoring of the tip admittance in the supporting electrolyte alone (without added redox mediators) can provide sufficient feedback information for successful AC-SECM imaging of a nonconductive substrate.

AC-SECM imaging of mixed samples (containing conductive and nonconductive areas) was performed in a fixed-Z mode. Figure 9 shows an image of platinum gauze (100 mesh) made of 76 μm wires. Gaps between the wires were filled with Norland Optical Adhesive and the whole assembly was polished to expose the surface of the wires to solution; however, the wires were not connected to the external electrical circuit. Scanning was performed in a 1 mM solution of $NaClO_4$ with a 25 μm Pt tip electrode. AC modulation with frequency of 1880 Hz and amplitude of 350 mV (p-p) was used. The step size in the X and Y directions was 5 μm. It should be noted that, in Fig. 9, the regions with high admittance values correspond to exposed Pt wires.

Another scanning experiment involved a bimetallic electrode made of a 100 μm platinum disk surrounded by a gold ring (see Fig. 10). Imaging was performed at frequency 890 Hz and amplitude 100 mV p-p with a 25 μm Pt scanning tip. The base electrode was held at a constant potential of 25 mV and the tip bias was 225 mV. The step size in the X and Y directions was 5 μm. At each X,Y position, information about the phase and the modulus of the first and second harmonic of the AC current, as well as information about the DC current passing through the tip was recorded. In particular, images produced by the phase of the first harmonic (Fig. 11a) and the modulus of the second harmonic current (Fig. 11b) are interesting because they clearly show differences between gold and platinum.

Conclusions

It has been shown that the admittance of an ultramicroelectrode placed at a small distance from a solid/solution interface depends on the distance from the solid and/or on the interfacial properties of the solid. This allows imaging of solid substrates in solutions of electrolytes in the absence of redox mediators. In the case of conductive solids, a localized (first and second order) impedance characteristic of the substrate can be obtained as a function of potential. Quantitative interpretation of the first order impedance data may be difficult because of the complexity of the equivalent circuits. However, we believe that quantitative interpretation of the second order impedance data may be possible in the future. It should be noted that the second order response (in other words the second harmonic current and the faradaic rectification) is almost exclusively generated by faradaic charge transfer processes that occur at the tip and at the base electrode. The contribution from the tip is constant during a measurement, but the contribution from the base electrode varies depending on the spatial coordinates and on the base electrode potential.

References

1. Bard AJ, Fan FF, Kwak J, Lev O (1989) Anal Chem 61:132
2. Bard AJ, Mirkin MV (eds)(2001) Scanning electrochemical microscopy. Marcel Dekker, New York.

3. Bard AJ, Faulkner LR (2001) Electrochemical methods: fundamentals and applications, 2nd edn. Wiley, New York, p 669
4. Mirkin MV, Richards TC, Bard AJ (1993) J Phys Chem 97:7672
5. Zhou F, Bard AJ (1994) J Am Chem Soc 116:393
6. Kasai S, Yokota A, Zhou H, Nishizawa M, Niwa K, Onouchi T, Matsue T (2000) Anal Chem 72:5761
7. Kasai S, Hirano Y, Motochi N, Shiku H, Nishizawa M, Matsue T (2002) Anal Chim Acta 458:263
8. Lister TE, Pinhero PJ (2003) Electrochim Acta 48:2371
9. Horrocks BH, Schmidtke D, Heller A, Bard AJ (1993) Anal Chem 65:3605
10. Alpuche-Aviles MA, Wipf DO (2001) Anal Chem 73:4873
11. Ballesteros Katemann B, Schulte A, Calvo EJ, Koudelka-Hep M, Schuhmann W (2002) Electrochem Commun 4:134
12. Ballesteros Katemann B, Inchauspe CG, Castro PA, Schulte A, Calvo E J, Schuhmann W (2003) Electrochim Acta 48:1115
13. Etienne M, Schulte A, Schuhmann W (2004) Electrochem Commun 6:288
14. Galus Z (1994) Fundamentals of electrochemical analysis, 2nd edn. Ellis Horwood, New York, p 180
15. Bard AJ, Faulkner LR (2001) Electrochemical methods: fundamentals and applications, 2nd edn. Wiley, New York, p 640.
16. Engblom SO, Myland JC, Oldham KB, Taylor AL (2001) Electroanalysis 13:626
17. Slowinska K, Feldberg SW, Majda M (2003) J Electroanal Chem 555:61